PHYSICAL REVIEW D **82,** 016009 (2010)

Higgs boson searches and the $Hb\bar{b}$ coupling at the LHeC

Tao Han* and Bruce Mellado†

Department of Physics, University of Wisconsin, Madison, Wisconsin 53706, USA

(Received 15 September 2009; published 30 July 2010)

Once the existence of the Higgs boson is established at the CERN Large Hadron Collider (LHC), the focus will be shifted toward understanding its couplings to other particles. A crucial aspect is the measurement of the bottom Yukawa coupling, which is challenging at the LHC. In this paper we study the use of forward jet tagging as a means to secure the observation and to significantly improve the purity of the Higgs boson signal in the $H \to b\bar{b}$ decay mode from deep inelastic electron-proton scattering at the LHC. We demonstrate that the requirement of forward jet tagging in charged current events strongly enhances the signal-to-background ratio. The impact of a veto on additional partons is also discussed. Excellent response to hadronic shower and b-tagging capabilities are pivotal detector performance aspects.

DOI: 10.1103/PhysRevD.82.016009 PACS numbers: 11.15.Ex, 14.80.Bn

I. INTRODUCTION

In the standard model (SM) of electroweak interactions, the Higgs field is responsible for generating masses to all of the particles in the theory, the gauge bosons as well as the fermions. The observation of the Higgs boson is a priority at the Large Hadron Collider (LHC) [1] for the CMS [2,3] and ATLAS [4,5] experiments in order to test the mechanism for the electroweak gauge symmetry breaking. Once the existence of the Higgs boson is established, the focus will be shifted toward understanding its couplings to other particles, in particular, to the fermions. While it seems to be feasible to observe the production $gg \to H$ to indirectly test the $Ht\bar{t}$ coupling, and the decay $H \to \tau\bar{\tau}$ [6], the Yukawa couplings to other fermions remain very difficult to access at the LHC. A crucial aspect is the measurement of the bottom Yukawa coupling [7,8] since it is pivotal to check the consistency of the SM and beyond. Extensive studies have been performed over the years to assess the feasibility of this measurement [9–15]. Nevertheless, the observation of the $H \to bb$ decay remains challenging at the LHC [2,5].

Recently, there has been a consideration for high-energy ep collisions with the deep inelastic electron-nucleon scattering at the LHC (LHeC) [16]. The energy of the incoming proton is given by the LHC beam, and several scenarios are considered for the energy of the incoming electron as

$$E_p = 7 \text{ TeV}, \qquad E_e = 50\text{–}200 \text{ GeV}, \tag{1}$$

corresponding to the center of mass energies of $\sqrt{s} = 2\sqrt{E_p E_e} \approx 1.18$–$2.37$ TeV. The anticipated integrated luminosity is about the order of 10–100 fb^{-1} depending on the energy of the incoming electron and the design.

There will be a rich physics program at the LHeC [17]. Several studies have been reported recently regarding the feasibility of the observation of an SM Higgs boson with the decay mode $H \to b\bar{b}$ [17,18]. The prospects for observing this channel at the LHeC are very exciting. By combining this measurement with the observation of $H \to WW^\star, \tau\tau$ channels from the LHC we can expect to directly extract the bottom Yukawa coupling. In this paper we explore this aspect in detail for the LHeC. We use the forward jet-tagging as a means to secure the feasibility of the observation by significantly improving the purity of the Higgs boson signal. The implications of a central jet veto are also discussed. The Higgs boson signal efficiency is studied as a function of the energy of the incoming electron. The impact of the most relevant aspects of the detector performance is evaluated.

In Sec. II we briefly summarize the characteristics of the Higgs boson production in ep collisions for both the charged current (CC) and neutral current (NC) processes. In Sec. III A we give a description of the background processes considered here. In Sec. III B we quantify signal and background yields after the requirement of forward parton tagging. Results are summarized in Sec. V.

II. HIGGS BOSON PRODUCTION IN HIGH-ENERGY ep COLLISIONS

The leading production mechanism for the SM Higgs boson at the LHeC is

$$eq \to \nu_e H q' \quad \text{and} \quad eq \to eHq, \tag{2}$$

via vector boson fusion processes (VBF), as depicted in Fig. 1. It is remarkable that the Higgs boson production via VBF was first calculated for lepton-nucleon interactions [19–23]. Kinematic features of the signal were explored in [24,25].

*than@hep.wisc.edu
†bmellado@wisc.edu

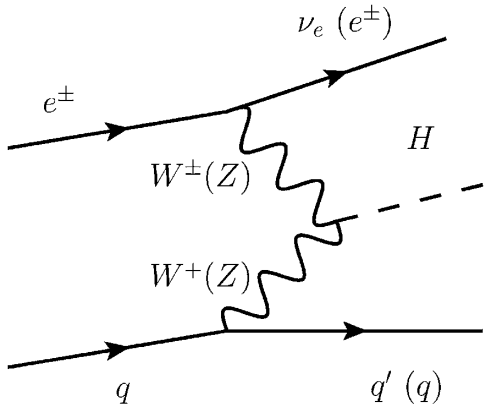

FIG. 1. Leading order diagram for the production of a standard model Higgs boson in ep collisions for the charged current and neutral current processes.

We first present the total cross sections in ep collisions as a function of the center of mass energy and the Higgs boson mass M_H without any acceptance cuts. Figure 2 displays the dependence of the cross section (a) on the Higgs boson mass and (b) on the energy of the incoming electron. We see that the production rate for the CC process (solid curves) is larger than that of the NC process (dotted curves) by about a factor of 4–6. This is mainly due to the accidentally suppressed NC coupling to the electrons. Here we have used the package MadGraph [26] for the full matrix element calculations at tree-level, and adopted the parton distribution functions CTEQ6L1 [27]. We choose the renormalization and factorization scales to be at the W-mass, which characterizes the typical momentum transfer for the signal processes.

In order to appreciate the unique kinematics of the VBF process it is most intuitive to express the cross section in a factorized form. Consider a fermion f of a center of mass energy E radiating a gauge boson V ($s \gg M_V^2$), the cross section of the scattering $fa \to f'X$ via V exchange can be expressed as

$$\sigma(fa \to f'X) \approx \int dx dp_T^2 P_{V/f}(x, p_T^2)\sigma(Va \to X) \quad (3)$$

where $\sigma(Va \to X)$ is the cross section of the $Va \to X$ scattering and $P_{V/f}$ can be viewed as the probability distribution for a weak boson V of energy xE and transverse momentum p_T. The dominant kinematic feature is a nearly collinear radiation of V off f, often called the "effective W-approximation" [28–30]. When the center of mass energy is much greater than the mass of the weak bosons, the probability distributions of the weak bosons with different polarizations can be approximated by

$$P_{V/f}^T(x, p_T^2) = \frac{g_V^2 + g_V^2}{8\pi^2} \frac{1 + (1-x)^2}{x} \frac{p_T^2}{(p_T^2 + (1-x)M_V^2)^2} \quad (4)$$

$$P_{V/f}^L(x, p_T^2) = \frac{g_V^2 + g_V^2}{4\pi^2} \frac{1-x}{x} \frac{(1-x)M_V^2}{(p_T^2 + (1-x)M_V^2)^2}. \quad (5)$$

These expressions lead us to the following observations:

(1) Unlike the QCD partons that scale like $1/p_T^2$ at the low transverse momentum, the final state quark f' typically has $p_T \sim \sqrt{1-x}M_V \leq M_W$.

(2) Because of the $1/x$ behavior for the gauge boson distribution, the outgoing parton energy $(1-x)E$ tends to be high. Consequently, it leads to an energetic forward jet with small, but finite, angle with respect to the beam.

(3) At high p_T, $P_{V/f}^T \sim 1/p_T^2$ and $P_{V/f}^L \sim 1/p_T^4$, and thus the contribution from the longitudinally polarized gauge bosons is relatively suppressed at high p_T to that of the transversely polarized.

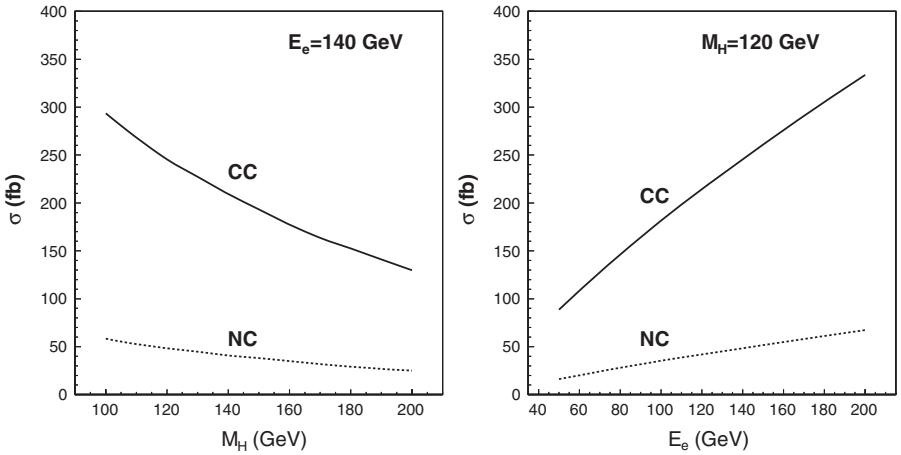

FIG. 2. Total cross sections, in fb, for the SM Higgs boson production in ep collisions at the LHeC for both CC (solid curves) and NC (dashed curves) processes. The plot on the left (a) shows the mass dependence for a fixed value of the energy of the incoming electron, $E_e = 140$ GeV. The plot on the right (b) displays the E_e dependence for a fixed Higgs boson mass, $M_H = 120$ GeV.

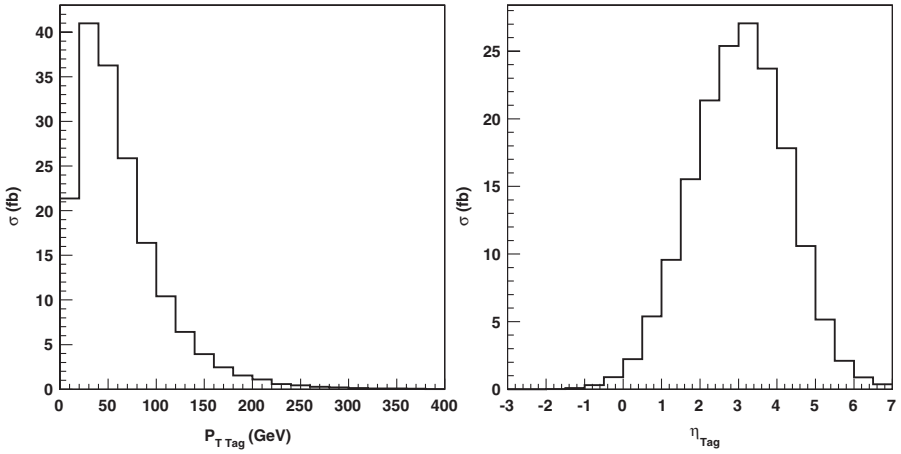

FIG. 3. Kinematic distributions for the forward parton (j) in units of fb per bin for the process $e^- p \to \nu_e H j$. The plot on the left (a) is for the transverse momentum distribution, and that on the right (b) shows the pseudorapidity distribution.

These features are illustrated in Fig. 3, where the plots on the left and right display the transverse momentum and pseudorapidity distributions of the outgoing jet (j), respectively, for the process of $e^- p \to \nu_e H j$. Here and henceforth, for illustration, we have taken the parameters as

$$E_p = 7 \text{ Tev}, \qquad E_e = 140 \text{ GeV}, \qquad M_H = 120 \text{ GeV}. \tag{6}$$

Supported by these figures, items 1 and 3 clearly motivate a tagging for a forward jet to separate the QCD backgrounds [31,32], while item 3 suggests a veto of central jets with high p_T to suppress the backgrounds initiated from the transversely polarized gauge bosons, and from other high p_T sources such as top quarks [33].

Large samples of events were generated with the Madgraph package without making the effective W-approximation. The branching fraction to $b\bar{b}$ is obtained with HDECAY [34] and it is equal to 0.677 for $M_H = 120$ GeV. The kinematics of the Higgs boson decays are handled by the decay interface of the Madgraph package.

We are also tempted to consider the process of the double Higgs boson production $e^- p \to \nu_e H H j + X$. With the same settings as for the single Higgs boson production in Eq. (6), the cross section is about 0.05 fb. With an increase of the energy of the incoming electron to 500 GeV the cross section would increase to 0.3 fb. The rather small cross section makes a signal observation difficult. In particular, it renders setting meaningful limits on the trilinear Higgs boson self-coupling extremely challenging. We will thus not consider this double Higgs boson process further in this work.

III. CHARGED CURRENT SIGNAL

Because of the large production rate, we focus on the Higgs boson production signal via the charged current (CC) process in Eq. (2). The signal topology consists of large missing transverse energy (E_T^{miss}), a forward energetic jet, and $b\bar{b}$ from the Higgs decay.

A. Background processes

The two groups of leading backgrounds under consideration are the charged current background, and the photo-production. The CC processes considered are generically expressed as

$$e^- p \to \nu_e \qquad qq' \qquad j + X. \tag{7}$$

These include contributions from subprocesses $Wg \to t\bar{b}$, qq'; $WW \to b\bar{b}$; $WZ/\gamma^* \to qq'$ etc. The photo-production processes considered are

$$e^- p \to e^- \qquad qq' \qquad j + X. \tag{8}$$

They include the subprocesses $\gamma g \to b\bar{b}$; $t\bar{t}$ etc. We do not consider the neutral current backgrounds with momentum transfer $Q^2 > 1$ GeV. Because of the presence of a final state electron at a large angle, it is assumed that these events can be rejected by tagging the scattered electron and/or requiring cuts on the $E - p_Z$ in the event. We did not include photo-production backgrounds involving resolved photons. We do not expect that this process renders a leading background. Large missing transverse momentum thus arises in these processes primarily from mismeasurement of hadronic jets (see Sec. III B) and the leptonic decays of the W's.

Cross sections were calculated and events generated with the software package Madgraph [26]. The top quark and W-boson decays were handled by the decay interface of the Madgraph package. The factorization and renormalization scales were set to the Z boson mass. We impose the following generator-level acceptance cuts:

$$p_T(j) > 15 \text{ GeV}, \qquad \Delta R > 0.4. \tag{9}$$

A summary of the cross sections is given in the first row of Table I.

TABLE I. Cross sections (in fb) for signal and main background processes with the generator-level cuts as in Eq. (9) (first row) and the event selection cuts presented in Sec. III B. The last column displays the resulting signal-to-background ratios.

		CC		Photo-prod.			
Cuts	Higgs	$t\bar{b}$	$b\bar{b}j$	jjj	$b\bar{b}j$	$t\bar{t}$	S/B
Generator-level	170	3800	810	26000	48000	250	-
a	28	150	86	3.8	6.9	2.3	0.11
b	22	20	2.4	0.36	0.67	0.27	0.93
c	16	8.1	1.4	0.12	0.25	0.14	1.6
d	12	1.5	0.92	0.06	0.14	0.04	4.7

B. Event selection

Several experimental factors that contribute heavily to the feasibility of the Higgs boson search are considered here. First, in order to disentangle CC events from photo-production a good reconstruction of the missing transverse momentum is required. We evaluate the emergence of fake $E_T^{\rm miss}$ from mismeasurements of the energy of quark and gluons in the final state. This is performed by smearing the partonic energies with the hadronic energy relative resolution

$$\frac{\sigma_E}{E} = \frac{\alpha}{\sqrt{E}} \oplus \beta, \tag{10}$$

where we choose to take $\alpha = 0.6\ \text{GeV}^{1/2}$ and $\beta = 0.03$. These resolution parameters can be achieved by the reconstruction of hadronic jets in collider experiments [35]. The resolution of the invariant mass of the Higgs boson candidate without smearing the angular reconstruction of the hadronic jets is about 7%. Checks have been performed with different values of α and β; see the next subsection. The impact of hadronization and of the proton breakup on the $E_T^{\rm miss}$ reconstruction are not taken into account here. Although we emphasize the search for a Higgs boson in association with a forward parton, we adopt the same energy resolution as used above for other central jets.

The ability to tag hadronic jets from b-quarks with high efficiency while displaying strong rejections against hadronic jets arising from lighter quarks is also a crucial experimental aspect. We assume a b-jet tagging efficiency of

$$\epsilon_b = 60\% \text{ in the range } |\eta| < 2.5. \tag{11}$$

The fake rejection factors of 10 and 100 are taken for c-jet and light jets, respectively.

C. CC production

The leading background to our Higgs signal are the charged current processes as in Eq. (7). The following event selection is chosen[1]:

(a) Require the presence of two b-partons with $p_T > 30$ GeV in the pseudorapidity range $|\eta| < 2.5$. The two b-partons constitute a Higgs boson candidate. To suppress photo-production backgrounds a cut on the missing transverse momentum, $E_T^{\rm miss} > 25$ GeV, is required. The minimum difference in azimuthal angle between the observed $E_T^{\rm miss}$ and the three partons in the event is required to be greater than 0.2 rad. At this stage a charged lepton (e, μ, τ) veto with $p_T > 10$ GeV in the range $|\eta| < 2.5$ is applied.

(b) The invariant mass of the two b-partons is required to be within 10 GeV of the Higgs boson mass.

(c) It is required that the leading remaining parton in the event have $p_T > 30$ GeV and be found in the range $1 < \eta < 5$. This parton is referred to as the forward tagging parton.

(d) The invariant mass of the Higgs boson candidate and the forward tagging parton, $M_{HJ} > 250$ GeV [36].

Figure 4 displays the pseudorapidity distributions for the forward tag parton after the application of Cuts a-b. The solid histogram corresponds to the Higgs boson signal. The kinematics of the forward tag parton in the signal resemble that of the Higgs boson simulated for VBF in pp collisions. The forward tag parton points predominantly along the direction of the incoming proton. The dotted and dashed histograms correspond to the forward tag parton for the two leading background processes. The forward tag parton due to the process $e^- p \to \nu_e t\bar{b} + X$ arises from the decay of the W boson, which is predominantly produced centrally. The kinematics arising from CC production of Z bosons differs qualitatively due to the presence of transversely polarized W's. In this case the momentum transfer at the fWf' vertex is significantly larger, and therefore, the scattered quark is more central than in the case of the Higgs boson. For the same reason the observed $E_T^{\rm miss}$ is significantly larger in this process.

Figure 5 shows the distribution of the invariant mass of the Higgs boson candidate and the forward tag parton. The solid, dotted and dashed histograms correspond to the Higgs boson signal, $e^- p \to \nu_e t\bar{b} + X$, $e^- p \to \nu_e b\bar{b}j + X$ processes, respectively. The same discussion mentioned for Fig. 4 applies here. The variable shown in

[1]The event selection shown here is not the result of an optimization procedure.

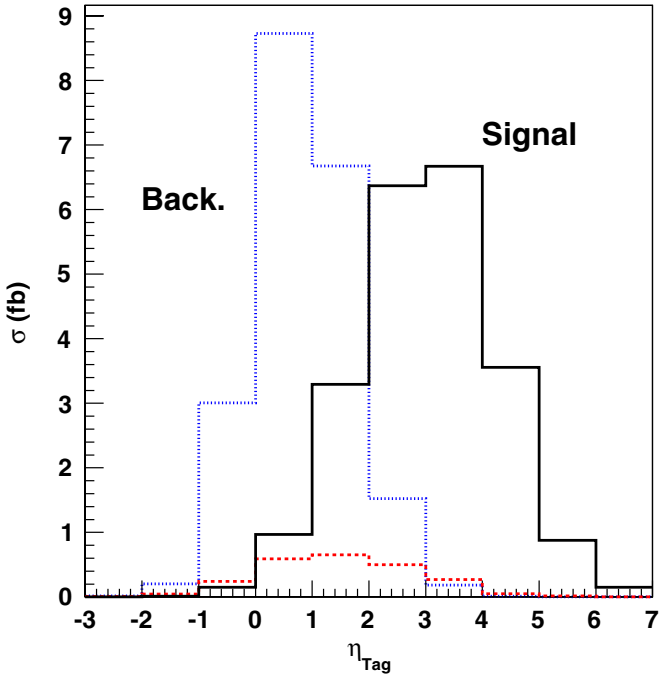

FIG. 4 (color online). Pseudorapidity distribution of the forward tag parton after the application of Cuts *a*-*b* (see Sec. III B). The solid, dotted and dashed histograms correspond to the Higgs boson signal, $e^- p \to \nu_e t\bar{b} + X$, $e^- p \to \nu_e b\bar{b}j + X$ processes, respectively. Results are given in units of fb per bin.

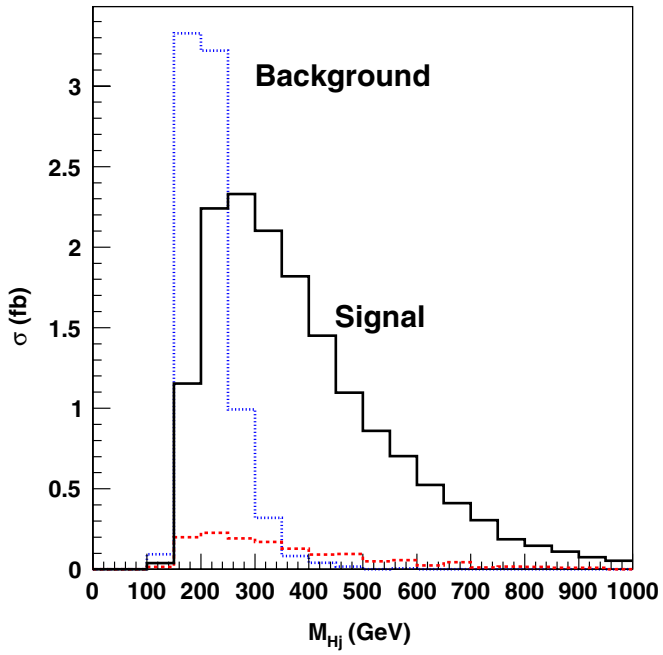

FIG. 5 (color online). Distribution of the invariant mass of the Higgs boson candidate and the forward tag parton after the application of Cuts *a*-*c* (see Sec. III B). The solid, dotted and dashed histograms correspond to the Higgs boson signal, $e^- p \to \nu_e t\bar{b} + X$, $e^- p \to \nu_e b\bar{b}j + X$ processes, respectively. Results are given in units of fb per bin.

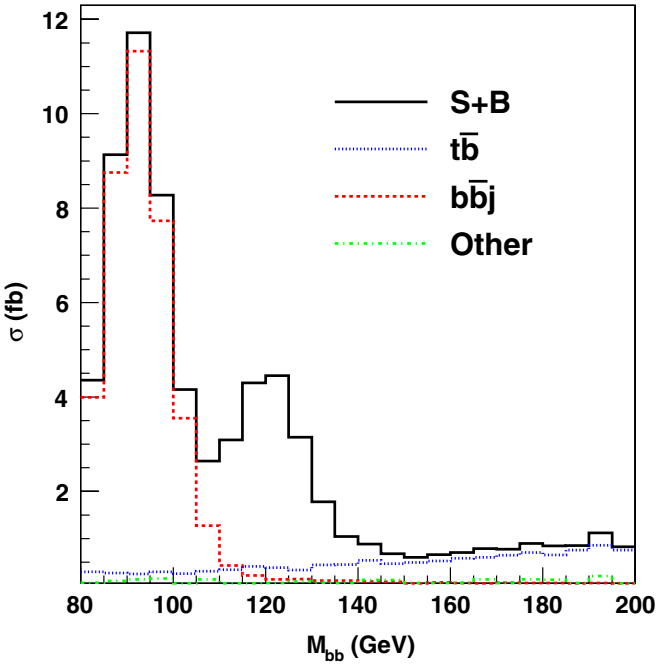

FIG. 6 (color online). Invariant mass spectrum of the Higgs boson candidate after the application of Cuts *a* and *c*-*d* (see Sec. III B). The black histogram corresponds to the sum of the signal and background processes. The contribution from the different background processes is given in separate histograms (see text). Results are given in units of fb per bin.

Fig. 5 is particularly effective in suppressing the $e^- p \to \nu_e t\bar{b} + X$ process.[2]

Figure 6 presents the invariant mass spectrum of the Higgs boson candidates after the application of Cuts *a* and *c*-*d* (excluding Cut *b*). The solid histogram in Fig. 6 corresponds to the sum of the signal and background processes. The contribution from the two leading backgrounds, $e^- p \to \nu_e W^- b\bar{b} + X$, $e^- p \to \nu_e b\bar{b}j + X$, is given by the dark dotted and dashed histograms, respectively. The total contribution from the rest of the processes is given by the light dotted histogram.

Table I displays the predicted cross sections (in fb) for signal and the main backgrounds after the application of the various cuts discussed above. The last column of Table I illustrates the significant enhancement of the signal-to-background ratio after the application of Cuts *c*-*d*. It is important to note that the background efficiencies for some of the backgrounds are reported here after requiring the presence of an additional parton with a p_T cut. Therefore the signal-to-background ratios reported after Cuts *a*-*b* are not representative of those for a purely in-

[2]In this process the pseudorapidity difference between the Higgs boson candidate and the forward tag parton is significantly smaller than that of the signal. However, the invariant mass of the forward tag parton and the Higgs boson candidate remains a better discriminator.

clusive analysis. For instance, the cross section of the photo-production process $e^- p \to e^- b\bar{b} + X$ after application of Cuts *a*-*b* is about 3.5 times larger than that of the photo-production process $e^- p \to e^- b\bar{b}j + X$ with the generator cuts specified in Sec. III A.

The impact of the central jet veto on the signal production is also considered here. We evaluate the additional suppression power of imposing a veto on events with additional partons in top-quark related backgrounds. In the processes $e^- p \to W^- b\bar{b} + X$ and $e^- p \to e^- t\bar{t} + X$ the forward tag parton comes from the decay of the W boson, which implies the presence of another parton in the event. By imposing a veto on events with an additional parton with $p_T > 30$ GeV in the range $|\eta| < 5$ the two backgrounds drop by 40% and 50%, respectively. The loss of signal efficiency is about 7%.

It is important to evaluate the dependence of the Higgs boson signal efficiency on the energy of the incoming electron. Table II gives a summary of the Higgs boson signal efficiencies for different values of E_e. The first rows correspond to the cumulative efficiencies and the second rows show the efficiencies for that cut with respect to the previous cut. The transverse momenta of the Higgs boson, its decay products and the forward tag parton do not depend strongly on E_e. The lower the energy is, the larger the longitudinal boost acquired by the Higgs boson, and, therefore, the decay products become more forward in the laboratory frame. This explains most of the loss of signal efficiency after Cut *a* as E_e decreases. As E_e decreases, the gauge boson off the quark line needs to be more energetic to produce a Higgs boson and the accompanying forward parton carries less energy. Also, the Higgs boson and the forward parton appear closer to each other in the laboratory frame and their invariant mass decreases at a lower E_e. This is illustrated by the E_e dependence of the signal efficiencies after Cut *d* with respect to that after Cut *c*. A similar effect is expected in the relevant background processes. Overall, the efficiency of the signal has a tendency to decrease as E_e decreases for $E_e < 100$ GeV, where for $E_e > 100$ GeV the dependence on E_e is not significant.

TABLE II. Higgs boson signal efficiencies for different energies of the incoming electron (in GeV) using the event selection chosen in Sec. III B. The first rows correspond to the cumulative efficiencies. The second rows show the efficiencies with respect to the previous cut.

Cut	$E_e = 50$	$E_e = 100$	$E_e = 140$	$E_e = 200$
a	0.129	0.157	0.166	0.171
	...	...	...	...
b	0.109	0.127	0.132	0.136
	0.84	0.81	0.80	0.80
c	0.076	0.090	0.093	0.095
	0.70	0.71	0.70	0.70
d	0.050	0.067	0.073	0.078
	0.66	0.75	0.79	0.82

The optimal value of the center of mass energy will depend on the expected integrated luminosity. The signal yield (cross section times signal efficiency) for $E_e = 140$ GeV is over a factor of 2 greater than that of $E_e = 70$ GeV. However, if the integrated luminosity at lower energies is significantly greater than that at larger energies it may be beneficial to consider lower energies.

A check was performed with a degraded scenario for the hadronic energy resolution as in Eq. (10), $\alpha = 0.7$ GeV$^{1/2}$ and $\beta = 0.05$. The relative resolution on the reconstructed Higgs boson mass degrades to 9%. The signal efficiency in the mass window degrades by 17% while the three leading backgrounds increase substantially. The contribution from the photo-production process $e^- p \to b\bar{b}j + X$ increases by about an order of magnitude and that of the process $e^- p \to \nu_e b\bar{b}j + X$ by almost a factor of 2. Overall, the signal-to-background ratio degrades by about a factor of 2. This indicates that the hadronic energy resolution is an essential element of the detector performance.

High performance of *b*-tagging is crucial for the robustness of the Higgs boson search. The fake backgrounds considered here come from the process $e^- p \to \nu_e jjj + X$ for which the final estate is composed of an admixture of light quarks and *c*-jets. With the fake rejection assumed here this background, which is dominated by *c*-quark fakes, constitutes less than 5% of the total background. The analysis could be optimized with a looser *b*-tagging efficiency without incurring in a significant increase of the total background.

The impact of the extension of the acceptance of the tracking system is evaluated. The increase of the tracking acceptance to $|\eta| < 3$ enhances the signal yield by about 6% while reducing the signal-to-background ratio by about 4%. A further increase of the tracking acceptance to $|\eta| < 3.5$ enhances the signal yield by only 1.5%.

IV. NEUTRAL CURRENT SIGNAL

The NC process has the advantage that the electron reconstruction is superior with respect to that of the missing neutrino in the CC process. However, it is not background-free. Furthermore, the NC process has a significantly smaller cross section with respect to the CC process as seen in Fig. 2.

The leading background arises from $e^- p \to e^- b\bar{b}j + X$, largely from the reactions $\gamma/Z\, g \to b\bar{b}$. To evaluate the signal-to-background ratio, we exploit the following acceptance cuts. We demand the existence of a backward electron and a pair of *b* quarks

$$\begin{aligned} p_T(e) &> 30 \text{ GeV}, \qquad |\eta_e| < 5, \\ p_T(b) &> 30 \text{ GeV}, \qquad |\eta_b| < 2.5. \end{aligned} \tag{12}$$

The invariant mass of the *b*-quarks is required to be in the same mass window as that considered in Sec. III C. We also require a forward parton in

$$p_T(j) > 30 \text{ GeV}, \qquad |\eta_j| < 5. \tag{13}$$

Assuming the same b-jet-tagging efficiency as used in Sec. III C and selecting the $b\bar{b}$ events within the Higgs mass window as before, the signal and background cross sections are 5.7 fb and 23.7 fb, respectively, leading to a signal-to-background ratio of about 0.25. This may yield a 4σ statistical significance for the signal with an integrated luminosity of 10 fb^{-1}. The application of a cut on M_{HJ} will improve the signal-to-background ratio, but at some cost of signal rate.

We consider that the Higgs boson search using the NC production mechanism is an interesting prospect, as it has the potential to enhance the overall Higgs boson signal efficiency. More studies would be required to evaluate the sensitivity due to this final state.

Before ending this section, we would like to make one remark. There is an interesting proposal at the LHC to search for the Higgs signal via the diffractive process $pp \to ppH$ [37]. Although the production cross section for this process is not well understood, the kinematics is very contained and this has the best chance to reconstruct the Higgs boson mass.

V. CONCLUSIONS

At the dawn of the LHC era, it is well motivated to consider the physics potential for the proposed proton-electron collider, the LHeC. We studied the use of forward jet tagging as a means to secure the observation of the Higgs boson in the $H \to b\bar{b}$ decay mode, and to significantly improve the purity of the signal. An excellent signal-to-background ratio of almost a factor of 5 can be achieved for the CC process while allowing for a significant rate of Higgs boson events. With this we believe that a measurement of the bottom Yukawa coupling at the LHeC may be feasible by means of combining the knowledge from the LHC on $H \to WW^{\star}, \tau\tau$.

The implications of a veto on additional partons were explored. It was demonstrated that the t-quark related backgrounds can be further reduced by about a factor of 2 with a signal loss of about 7%.

The dependence of the signal kinematics on the energy of the incoming electron were evaluated. Overall, the efficiency of the signal has a tendency to decrease as E_e decreases for $E_e < 100$ GeV, where for $E_e > 100$ GeV the dependence on E_e is not significant.

Two detector performance aspects have been identified as essential to the Higgs boson search: hadronic energy resolution and b-tagging capabilities. When considering a more conservative scenario for the hadronic energy resolution the signal-to-background ratio in the Higgs boson search degrades by a factor of 2. Large signal-to-background ratios can only be achieved with adequate b-tagging capabilities.

We also considered the isolation of the Higgs boson using the NC production mechanism. Although with a much smaller signal cross section and substantial backgrounds, we demonstrated that this has the potential to enhance the overall Higgs boson signal observation.

Because of the small di-Higgs boson cross-sections, setting meaningful limits on the trilinear Higgs boson self-coupling is extremely challenging in the range of energies of ep collisions considered here.

A simple cut-based analysis was performed here. More complex discriminators could be constructed in order to enhance the efficiency of the Higgs boson signal.

ACKNOWLEDGMENTS

We would like to thank J. Alwall and F. Maltoni for their invaluable help with the Madgraph package, and A. de Roeck, T. Vickey, and D. Zeppenfeld for discussions. This work was supported in part by the DoE Grant No. DE-FG02-95ER40896. The work of B. M. is also supported by the Wisconsin Alumni Research Foundation.

[1] L. Evans, P. Bryant *et al.*, JINST **3**, S08001 (2008).
[2] C. Collaboration, CERN Report No. CERN/LHCC 2006-021.
[3] R. Adolphi *et al.* (CMS), JINST **03**, S08004 (2008).
[4] G. Aad *et al.* (ATLAS), JINST **3**, S08003 (2008).
[5] G. Aad *et al.* (The ATLAS Collaboration), arXiv:0901.0512.
[6] D. L. Rainwater, D. Zeppenfeld, and K. Hagiwara, Phys. Rev. D **59**, 014037 (1998).
[7] D. Zeppenfeld, R. Kinnunen, A. Nikitenko, and E. Richter-Was, Phys. Rev. D **62**, 013009 (2000).
[8] M. Duhrssen *et al.*, Phys. Rev. D **70**, 113009 (2004).
[9] E. Richter-Was and M. Sapinski, Acta Phys. Pol. B **30**, 1001 (1999).
[10] V. Drollinger, T. Muller, and D. Denegri, arXiv:hep-ph/0111312.
[11] F. Maltoni, K. Paul, T. Stelzer, and S. Willenbrock, Phys. Rev. D **64**, 094023 (2001).
[12] V. Drollinger, T. Muller, and D. Denegri, arXiv:hep-ph/0201249.
[13] M. L. Mangano, M. Moretti, F. Piccinini, R. Pittau, and A. D. Polosa, Phys. Lett. B **556**, 50 (2003).
[14] E. Gabrielli *et al.*, Nucl. Phys. **B781**, 64 (2007).
[15] J. M. Butterworth, A. R. Davison, M. Rubin, and G. P. Salam, Phys. Rev. Lett. **100**, 242001 (2008).
[16] J. B. Dainton, M. Klein, P. Newman, E. Perez, and F. Willeke, JINST **1**, P10001 (2006).
[17] U. Klein, *Higgs Production at the lhec, DIS 2009, Madrid*.

[18] M. Ishitsuka, *Higgs Production at the lhec, DIS 2009, Madrid*.
[19] J. R. Ellis, M. K. Gaillard, and D. V. Nanopoulos, Nucl. Phys. **B106**, 292 (1976).
[20] J. M. LoSecco, Phys. Rev. D **14**, 1352 (1976).
[21] R. M. Godbole, Phys. Rev. D **18**, 95 (1978).
[22] Z. Hioki, S. Midorikawa, and H. Nishiura, Prog. Theor. Phys. **69**, 1484 (1983).
[23] T. Han and H. C. Liu, Z. Phys. C **28**, 295 (1985).
[24] G. Grindhammer, D. Haidt, J. Ohnemus, J. Vermaseren, and D. Zeppenfeld, in *Proc. of Large Hadron Collider Workshop, Aachen, Germany* (CERN-90-10-V-1, ECFA-90-133-V-1, 1990).
[25] J. Blumlein, G. J. van Oldenborgh, and R. Ruckl, Nucl. Phys. **B395**, 35 (1993).
[26] J. Alwall *et al.*, J. High Energy Phys. 09 (2007) 028.
[27] J. Pumplin *et al.*, J. High Energy Phys. 07 (2002) 012.
[28] R. N. Cahn and S. Dawson, Phys. Lett. B **136**, 196 (1984).
[29] M. S. Chanowitz and M. K. Gaillard, Phys. Lett. B **142**, 85 (1984).
[30] G. L. Kane, W. W. Repko, and W. B. Rolnick, Phys. Lett. B **148**, 367 (1984).
[31] R. Kleiss and W. J. Stirling, Phys. Lett. B **200**, 193 (1988).
[32] V. D. Barger, T. Han, and R. J. N. Phillips, Phys. Rev. D **37**, 2005 (1988).
[33] V. D. Barger, K.-m. Cheung, T. Han, and R. J. N. Phillips, Phys. Rev. D **42**, 3052 (1990).
[34] A. Djouadi, J. Kalinowski, and M. Spira, Comput. Phys. Commun. **108**, 56 (1998).
[35] C. Amsler *et al.* (Particle Data Group), Phys. Lett. B **667**, 1 (2008).
[36] B. Mellado, W. Quayle, and S. L. Wu, Phys. Lett. B **611**, 60 (2005).
[37] V. A. Khoze, A. D. Martin, and M. G. Ryskin, Phys. Lett. B **650**, 41 (2007).